Supplemental Material for "Unconventional quantum sound-matter interactions in spin-optomechanical-crystal hybrid systems"

Xing-Liang Dong,[1] Peng-Bo Li,[1,2,*] Tao Liu,[2,3] and Franco Nori[2,4]

[1] *MOE Key Laboratory for Nonequilibrium Synthesis and Modulation of Condensed Matter, Shaanxi Province Key Laboratory of Quantum Information and Quantum Optoelectronic Devices, School of Physics, Xi'an Jiaotong University, Xi'an 710049, China*

[2] *Theoretical Quantum Physics Laboratory, RIKEN Cluster for Pioneering Research, Wako-shi, Saitama 351-0198, Japan*

[3] *School of Physics and Optoelectronics, South China University of Technology, Guangzhou 510640, China*

[4] *Department of Physics, The University of Michigan, Ann Arbor, Michigan 48109-1040, USA*

In this Supplemental Material, we first present more details on the optomechanical systems, including band properties versus related parameters, an accurate full-wave simulation for the optomechanical system, and the realization of lasers with position-dependent phases. The disorders in the optical and mechanical frequencies are considered as well. Second, we discuss the properties of SiV centers and their strain coupling to the acoustic modes in optomechanical crystals. Third, we introduce the master equation for the study of the Markovian dynamics of the system. Fourth, we take a discussion of quasi-chiral sound-matter interactions and one of the applications in quantum information processing, i.e., entangled state preparation. Finally, we present more details on the photon-phonon bound states and odd-neighbor spin-spin interactions. In particular, we consider the bound states and exact dynamics of spin interactions in a finite optomechanical array.

OPTOMECHANICAL CRYSTALS

Properties of the band structure

The optomechanical Hamiltonian in the main text ($\hbar = 1$) is given by

$$\hat{H}_{\rm OM} = \Delta/2\sum_n \hat{a}_n^\dagger \hat{a}_n + \omega_M/2\sum_n \hat{b}_n^\dagger \hat{b}_n - G\sum_n e^{-in\theta}\hat{a}_n^\dagger \hat{b}_n - J\sum_n \hat{a}_{n+1}^\dagger \hat{a}_n - K\sum_n \hat{b}_{n+1}^\dagger \hat{b}_n + \text{H.c.}. \tag{S1}$$

In the Fourier basis, it has the form of

$$\hat{H}(k) = \begin{pmatrix} -2J\cos(k-\theta) & -G \\ -G & -2K\cos(k) \end{pmatrix}, \tag{S2}$$

which shows a phonon with momentum k is coupled to a photon with momentum $k-\theta$. The eigenmodes are polaritons composed of photons and phonons. We diagonalize the Hamiltonian by a unitary transformation

$$P_k = \begin{pmatrix} -\sin\theta_k & \cos\theta_k \\ \cos\theta_k & \sin\theta_k \end{pmatrix}, \tag{S3}$$

with $\sin^2\theta_k = G^2/[G^2 + (\omega_l(k) + 2K\cos(k))^2]$ the weight of photons (phonons) in upper (lower) band, and $\cos^2\theta_k = G^2/[G^2 + (\omega_u(k) + 2K\cos(k))^2]$ the weight of phonons (photons) in upper (lower) band. After diagonalization, the dispersions in the first Brillouin zone are

$$\omega_{u/l}(k) = -J\cos(k-\theta) - K\cos(k) \pm \sqrt{(K\cos(k) - J\cos(k-\theta))^2 + G^2}. \tag{S4}$$

Note that $\omega_u(k\pm\pi) = -\omega_l(k)$ and $\cos^2\theta_{k\pm\pi} = \sin^2\theta_k$. These can be understood intuitively from the fact that the bare photonic and phononic bands are cosine functions and $\cos(k\pm\pi) = -\cos(k)$. The parameter θ breaks the time-reversal symmetry, that is, $\omega_{u/l}(k) \neq \omega_{u/l}(-k)$.

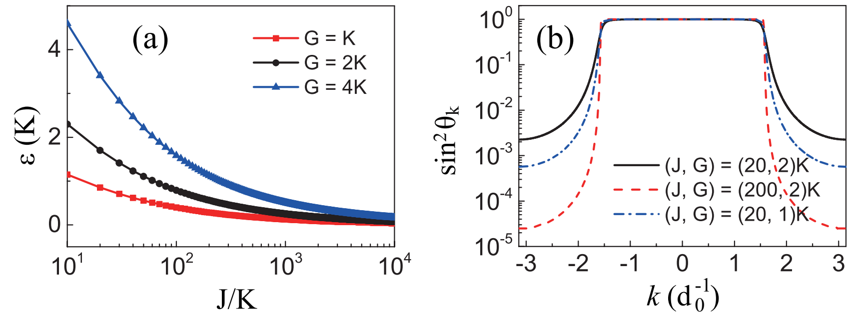

FIG. S1. (Color online) (a) The size of the gap ε versus the ratio J/K with $G = 1K$, $2K$ and $4K$. (b) The weights of photons composing polaritons in the upper band for $(J, G) = (20, 2)K$ in black solid line, $(J, G) = (200, 2)K$ in red dash line and $(J, G) = (20, 1)K$ in blue dash dot line. Here, $\theta = \pi$.

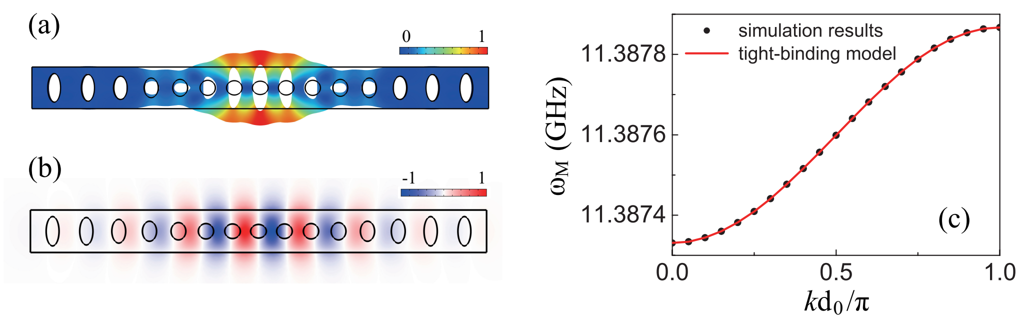

FIG. S2. (Color online) Finite-element (FEM) simulations of a single diamond optomechanical nanocavity, which co-localizes (a) a phononic mode (displacement field $|Q|/|Q_{max}|$) and (b) an optical mode (y component of electric field $E_y/|E_{y\ max}|$). The frequencies are $\omega_M/2\pi \sim 11.4$ GHz and $\omega_c/2\pi \sim 250$ THz. (c) The phononic band close to the localized mode. The dots indicate the simulation results and the solid line is from the tight-binding model with the expression of $\omega_M(k)/2\pi = 11.387599 - 0.000268 \times \cos(kd_0)$ GHz.

The structure parameters K, J and laser driving parameters G, θ completely determine the size, shape and hybridization properties of the dispersions. In our scheme, we mainly consider the values of the phase gradient such that the bare mechanical band is bisected by the bare photon band. Since the effects of θ are discussed in the main text, we here focus on the parameters K, J, G. Actually, these parameters can impact the bandgap and the weights of photons and phonons composing the polaritons. Without loss of generality, we consider the parameter regime $\theta = \pi$. We plot the size of the bandgap ε ($\varepsilon = \varepsilon_1 + \varepsilon_2$ and $\varepsilon_1 = 0$) opened by the optomechanical interaction versus the ratio J/K with $G = 1K, 2K$ and $4K$ in Fig. S1(a). The bandgap decreases when increasing the value of J/K or decreasing the value of G. As a result, the tunability of θ is reduced and the system is more sensitive to the disorder which can close the bandgap. We also plot the weights of photon components of polaritons in the upper band for different values of J and G in Fig. S1(b). However, the result shows that the high purity of phonon-like excitations requires larger photons hopping rate and smaller optomechanical coupling strength. As a balance, we choose $J = 20K$ and $G = 2K$ in the main text such that the bandgap is large enough and $\sin^2\theta_k < 0.01$ can be easily satisfied.

Implementation of the optomechanical Hamiltonian

In this section, we simply discuss the implementation of the optomechanical system, where we consider an array of co-localized phononic and optical cavities formed in a diamond nanobeam and a tight-binding model is assumed for simplicity. In addition, a position-dependent phase is introduced for each optomechanical interaction through writing gradient phase in lasers. Using the finite-element (FEM) simulation package COMSOL, we present a full-

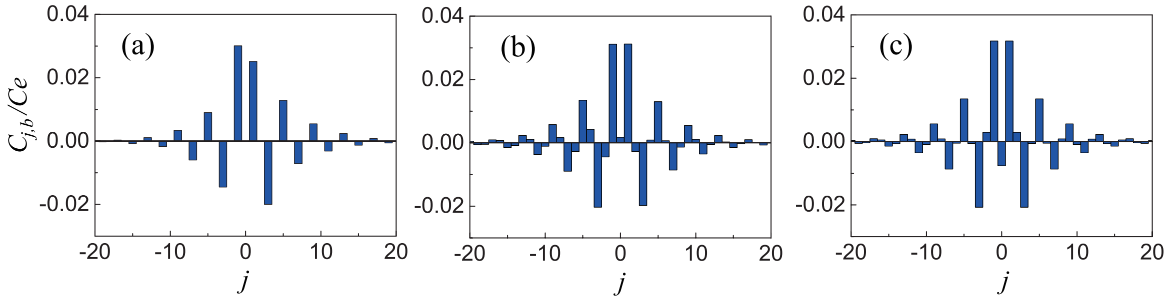

FIG. S3. (Color online)Wave function distribution of phonon bound state $C_{j,b}$ in real space with $\theta = \pi$ and $E_{\rm BS} = 0$. (a) Off-diagonal disorder in both optical and mechanical frequencies with strength $W_C = 0.5J$ and $W_M = 0.5K$. (b) On-site disorder in optical frequencies with strength $W_C = 0.5J$. Here, $J = 20K$, $G = 2K$ and $g_{\rm eff} = 0.08K$. (c) $E_{\rm BS} = 0.1\varepsilon$.

wave simulation for the optomechanical system in Fig. S2, with parameters of the nanocavity taken from related experimental work [1, 2]. In Fig. S2(a,b), we show the distribution of the displacement field $|Q|$ for localized mechanical modes and the y component of the electric field E_y for localized optical modes in a unit cell (defect nanocavity). The frequencies are around $2\pi \times 11.4$ GHz for mechanical breathing modes and $2\pi \times 250$ THz for optical modes. In Fig. S2(c), we compare the phononic dispersion near the localized mode with the result predicted from the tight-binding model and find a good agreement, which indicates the validity of the tight-binding approximation.

The position-dependent phase in laser drive can be implemented on chip. Here, we follow closely the supplementary materials in Ref. [3], which introduces a $1 \times N$ multi-mode interferometer to realize it. We use the $1 \times N$ multi-mode interferometer to divide the power equally to N optical fibers, which are evanescently coupled to N optomechanical nanocavities. The first method is to vary the length of the fibers such that the light propagating in different waveguides experiences different distances, thus acquiring a phase gradient. The second one is to use heated zero-loss resonators as all-pass filters to pick up phases which are related to resonators' resonance frequency tuned by temperature.

Disorder

We now consider the effects of the disorder on both the optical and mechanical frequencies, which arises from the fabrication imperfection and is the main experimental obstacle in optomechanical lattices. The on-site disorder can cause an additional localization, i.e., Anderson localization. As predicted in perturbation theory, the 1D chain with random disorders distributed in the interval $[-W/2, W/2]$ can have a localization length about $100J_c^2/W^2$ [4], where J_c is the hopping rate and W is the disorder strength. For the small disorder strength such that $W \lesssim J_c$, the localization length is hundred of sites, which can be much larger than the size of the array.

Moreover, we expect that if the disorder is large enough the focusing areas (gap and asymmetric area) will be smeared away. We roughly estimate the critical disorder strength by considering the two limits that all optical (acoustic) cavities have a frequency offset of $\pm W_C/2$ ($\pm W_M/2$). This will makes the photonic (phononic) band and consequently the focusing area be shifted up and down. Up to the specific value of W_C (W_M), the focusing areas of these two limiting cases have no overlap. This indicates that the focusing area starts to close in the presence of the disorder. We find this occurs when $W_C \sim J$ ($W_M \sim K$) in the case of $\varepsilon \sim K$, in line with the discussion in Ref. [5], where a topological acoustic bandgap is opened by optomechanical interactions.

As a example, we numerically give the bound state ($E_{\rm BS} = 0$) in the presence of off-diagonal and on-site disorder, which are shown in Fig. S3(a,b). We consider off-diagonal and on-site disorder by adding random terms $\sum_{n,\beta=a,b}(\xi_{n,\beta}\hat{\beta}_n^\dagger\hat{\beta}_{n+1} + \text{H.c.})$ and $\sum_n \xi_n \hat{a}_n^\dagger \hat{a}_n$ to Hamiltonian respectively. The disorder strength is chosen in the range $\xi \in [-W/2, W/2]$, with $W_C = J/2$ for optical frequencies and $W_M = K/2$ for mechanical frequencies. In particular, we show that the feature of alternating photon and phonon components of the bound state is robust against off-diagonal disorder. The numerical results are consistent with the analysis above.

In general, about 10^{-6} precision for optical frequencies and 10^{-3} precision for mechanical frequencies are enough to neglect the effects of the disorder, under the parameters considered in our system. Though it's challenge to fabricate such high-precision optical cavity array in experiment, the previous work have demonstrated that through some approaches such as post-fabrication fine-tuning techniques [6, 7], the required levels of accuracy can be reached.

SIV CENTERS

SiV center's level structure and its strain coupling to phononic modes in diamond crystal have been discussed in the previous work [8]. Here, for completeness, we make a simple discussion. SiV centers are point defects in diamond with a silicon atom lying in between two adjacent vacancies, whose electronic ground state is an unpaired hole of spin $S = 1/2$. In the present of spin-orbit coupling, the ground state is split into two branches with a gap of $\Delta_{\mathrm{SiV}}/2\pi \sim 46$ GHz. By further applying a magnetic field, each branches splits into two doublets, labeled as $\{|g\rangle = |e_- \downarrow\rangle, |e\rangle = |e_+ \uparrow\rangle\}$ and $\{|f\rangle = |e_+ \downarrow\rangle, |d\rangle = |e_- \uparrow\rangle\}$, as shown in Fig. 1. Here, $|e_\pm\rangle$ are eigenstates of the orbital angular momentum operator $\hat{L}_z|e_\pm\rangle = \pm|e_\pm\rangle$. We take the indirect coupling scheme via a Raman process for example. We drive SiV centers by microwave fields with the frequency ω_L and the pump strength Ω. Thus, the Hamiltonian of single SiV centers is obtained

$$\hat{H}_{\mathrm{SiV}} = \omega_B|e\rangle\langle e| + \Delta_{\mathrm{SiV}}|f\rangle\langle f| + (\omega_B + \Delta_{\mathrm{SiV}})|d\rangle\langle d| + [\Omega e^{i\omega_L t}(|g\rangle\langle d| + |e\rangle\langle f|) + \mathrm{H.c.}], \tag{S5}$$

where ω_B is the Zeeman energy.

On the other hand, local lattice distortions associated with internal compression modes of the optomechanical crystal affect the defect's electronic structure, which induces a strain coupling between these phonons and the orbital degrees of freedom of the center. The SiV-phonon coupling Hamiltonian is

$$\hat{H}_{\mathrm{strain}} = g_k(|g\rangle\langle f| + |e\rangle\langle d|)\hat{b} + \mathrm{H.c.}, \tag{S6}$$

with $\hat{b}$ the annihilation operator for the acoustic mode and g_k the coupling strength, which can be expressed as

$$g_k = \frac{d}{v}\sqrt{\frac{\hbar\omega_k}{2\rho V}}\xi(\vec{r}_{\mathrm{SiV}}). \tag{S7}$$

Here, $d/2\pi \sim 1$ PHz is the strain sensitivity, $v \sim 10^4$ m/s is the group velocity of acoustic wave in diamonds, $\omega_k \sim \Delta_{\mathrm{SiV}}$, $\rho \sim 3500$ kg/m^3, V is the volume of optomechanical nanocavity and $\xi(\vec{r}_{\mathrm{SiV}}) \sim 1$ is the strain distribution at SiV centers position. If we choose the size of cavities with length of several microns and cross section about 100 nm $\times$100 nm, the coupling strength can be calculated as $g_k/2\pi \sim 30$ MHz. This calculation is agreed with one in Ref. [8] using finite-element simulations.

When the Zeeman frequency ω_B is large enough, only the Raman channel $|g\rangle \to |f\rangle \to |e\rangle$ contributes. By dropping the high frequency oscillation items and the constant items, we can obtain the free Hamiltonian and effective SiV-phonon coupling Hamiltonian with many centers

$$\hat{H}_{\mathrm{free}} = \omega_0/2\sum_m(|e\rangle^m\langle e| - |g\rangle^m\langle g|) \tag{S8}$$

$$\hat{H}_{\mathrm{int}} = g_{\mathrm{eff}}\sum_m(|e\rangle^m\langle g|\hat{b}_{x_m} + \mathrm{H.c.}), \tag{S9}$$

where $\omega_0 = \omega_B + \omega_L$ is the transition frequency of single spins, $g_{\mathrm{eff}} = g_k\Omega/(\Delta_{\mathrm{SiV}} - \omega_0)$ is the effective spin-phonon coupling strength and x_m is the position of phonon cavity the mth spin coupled to. Lastly, we switch the effective interaction to the reciprocal space, in terms of polariton operators $\hat{u}_k$ and $\hat{l}_k$, it reads

$$\hat{H}_{\mathrm{int}} = \frac{g_{\mathrm{eff}}}{\sqrt{N}}\sum_{k,m}\hat{\sigma}_+^m e^{ikx_m}(\cos\theta_k\hat{u}_k + \sin\theta_k\hat{l}_k) + \mathrm{H.c.}, \tag{S10}$$

with $\hat{\sigma}_+^m = |e\rangle^m\langle g|$ the Pauli operator.

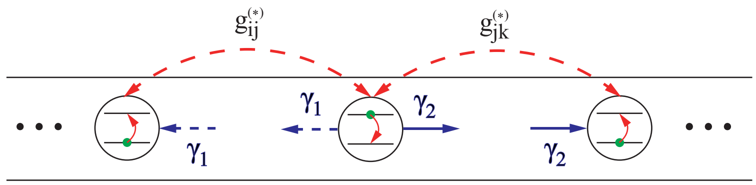

FIG. S4. (Color online) Schematic of resonant sound-matter interactions in the optomechanical crystal. The resonant spin-bath interactions are chiral, which is reflect by $\gamma_1 \neq \gamma_2$, with γ_1 and γ_2 the decay rate into the left- and right-moving reservoir modes. The band-edge-induced long-range interactions are also given.

MASTER EQUATION

Before the access to specific regimes for the study of sound-matter interactions, we first introduce an outstanding approach in quantum optics, i.e., master equation approach. This method allows us exploring the Markovian dynamics of system, where the degree of freedom of bath can be traced out [9]

$$\frac{d\hat{\rho}_s}{dt} = \sum_{i,j} \Gamma_{ij} (\hat{\sigma}_-^i \hat{\rho}_s \hat{\sigma}_+^j - \hat{\sigma}_+^j \hat{\sigma}_-^i \hat{\rho}_s) + \text{H.c.}, \tag{S11}$$

with the reservoir-mediated coupling between spins

$$\begin{aligned}\Gamma_{ij} &= \lim_{s\to 0^+} \sum_k \sum_{\alpha=u,l} \frac{\langle \text{vac}|\langle g|\sigma_-^j \hat{H}_{\text{int}} \alpha_k^\dagger \alpha_k \hat{H}_{\text{int}} \sigma_+^i |g\rangle|\text{vac}\rangle}{s - i(\omega_0 - \omega_\alpha(k))} \\ &= \lim_{s\to 0^+} \frac{g_{\text{eff}}^2}{2\pi} \int_{-\pi}^{\pi} dk e^{ikx_{ij}} \Big(\frac{\cos^2\theta_k}{s - i(\omega_0 - \omega_u(k))} + \frac{\sin^2\theta_k}{s - i(\omega_0 - \omega_l(k))} \Big).\end{aligned} \tag{S12}$$

By defining $\Gamma_{ij} = \gamma_{ij} + iJ_{ij}$, with

$$\begin{aligned}\gamma_{ij} &= \frac{1}{2}(\Gamma_{ij} + \Gamma_{ji}^*) \\ J_{ij} &= \frac{1}{2i}(\Gamma_{ij} - \Gamma_{ji}^*),\end{aligned} \tag{S13}$$

we arrive to the following expression with a separated coherent and incoherent parts

$$\frac{d\hat{\rho}_s}{dt} = -i \sum_{i,j} J_{ij} [\hat{\sigma}_+^j \hat{\sigma}_-^i, \hat{\rho}_s] + \sum_{i,j} \gamma_{ij} (2\hat{\sigma}_-^i \hat{\rho}_s \hat{\sigma}_+^j - \hat{\sigma}_+^j \hat{\sigma}_-^i \hat{\rho}_s - \hat{\rho}_s \hat{\sigma}_+^j \hat{\sigma}_-^i). \tag{S14}$$

BAND REGIME

Quasi-chiral spin dynamics

When the spins' frequency lies within the asymmetric area ε_1 in the main text, the dynamics of spins is dominated by band-edges as well as two resonant k-modes with opposite group velocity, leading to quasi-chiral sound-matter interactions. The chiral spin-spin interactions arise from the chiral spin-bath interaction that the possibility of spin decay into the left- and right-moving reservoir modes is unequal, which is shown in Fig. S4. To gain analytical intuition of this regime, we take the limit of weak spin-phonon coupling. The dynamics is determined by Eq. (S11). In contrast to the main text, where we divide Γ_{ij} into three parts, we now calculate Γ_{ij} directly. The Eq. (S12) can be unfolded as

$$\Gamma_{ij}(z) = \frac{ig_{\text{eff}}^2}{2\pi} \int_{-\pi}^{\pi} dk e^{ikx_{ij}} \frac{z + 2J\cos(k-\theta)}{z^2 + 2(J\cos(k-\theta) + t\cos(k))z + 4JK\cos(k-\theta)\cos(k) - G^2}, \tag{S15}$$

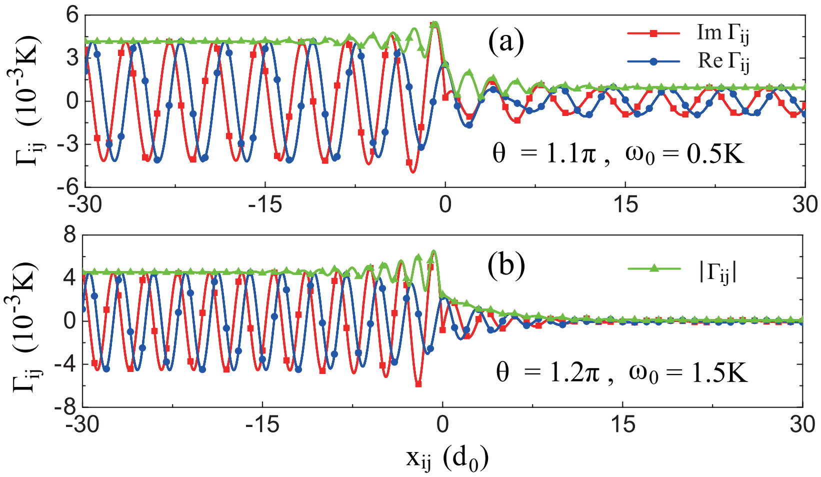

FIG. S5. (Color online) Collective coupling Γ_{ij} as a function of position x_{ij} with (a) $\omega_0 = 0.5K$, $\theta = 1.1\pi$ and (b) $\omega_0 = 1.5K$, $\theta = 1.2\pi$. In which, the symbols represent the values at lattice position. The parameters are $g_{\text{eff}} = 0.08K$, $J = 20K$ and $G = 2K$.

By means of the change of variable $y \equiv e^{ik}$ for $x_{ij} \geq 0$ and $y \equiv e^{-ik}$ for $x_{ij} < 0$, we can solve these integrals. Here, we take $x_{ij} \geq 0$ as a example

$$\Gamma_{ij}(z) = \frac{g_{\text{eff}}^2}{2\pi} \oint_{|y|=1} dy \frac{y^{x_{ij}}[yz + J(y^2 e^{-i\theta} + e^{i\theta})]}{ay^4 + by^3 + cy^2 + dy + e} = ig_{\text{eff}}^2 \sum_{|y_l|<1} \frac{y_l^{x_{ij}}[y_l z + J(y_l^2 e^{-i\theta} + e^{i\theta})]}{4ay_l^3 + 3by_l^2 + 2cy_l + d}, \tag{S16}$$

where we apply the Cauchy's residue theorem and define $a = e^* = JKe^{-i\theta}$, $b = d^* = z(Je^{-i\theta} + K)$, $c = z^2 - G^2 + 2JK\cos(\theta)$. The denominator is a quartic equation and the corresponding roots can be solved analytically or numerically. Finally, taking $z = \omega_0 + i0^+$ to the above equation and solving the integral in the interval $x_{ij} < 0$, we can obtain the required value of Γ_{ij}. We numerically plot Γ_{ij} as a function of x_{ij} with $\omega_0 = 0.5K$ and $\theta = 1.1\pi$ in Fig. S5(a), and with $\omega_0 = 1.5K$ and $\theta = 1.2\pi$ in Fig. S5(b). The function is continuous, where the symbols correspond to the values at lattice position. We find that, in a limited area $-15 \lesssim x_{ij} \lesssim 15$, the coupling strength is oscillating with a damped amplitude in the distance. Beyond this area, we observe the collective decay rates are oscillating with certain but different amplitudes and periods, $\Gamma_{ij} \approx \gamma_1 e^{ik_1 x_{ij}}$ and $\Gamma_{ij} \approx \gamma_2 e^{ik_2 x_{ij}}$ for respectively $x_{ij} \lesssim -15$ and $x_{ij} \gtrsim 15$. Here, $\gamma_1 = g_{\text{eff}}^2 \cos^2\theta_{k_1}/|v_g^1|$ and $\gamma_2 = g_{\text{eff}}^2 \cos^2\theta_{k_2}/|v_g^2|$, relating to the left ($v_g^1 < 0$) and right ($v_g^2 > 0$) propagating acoustic waves, with $\cos^2\theta_{k_{1,2}}$ the weights of phononic components of the polaritons in the upper band and $v_g^{1,2} = \partial\omega/\partial k|_{\omega=\omega_0, k=k_{1,2}}$ the group velocity. As discussed in the main text, the quasi-chiral interactions contain band-induced interaction part $\sum_{l=1,2} \gamma_l e^{ik_l x_{ij}} \Theta(x_{ij}/v_g^l)$, and band-edge-induced interaction part P.V.$\Gamma_{ij} \sim Ce^{-|x_{ij}|/\xi} e^{ikx_{ij}}$, which decays exponentially (see below). In particular, for the parameters used in Fig. S5(b), the value of γ_2 is small enough such that for $x_{ij} > 0$, $|\Gamma_{ij}| \approx |\text{P.V.}\Gamma_{ij}| \sim Ce^{-|x_{ij}|/\xi}$, i.e., the scaling of the self-energy is exponential decay.

Mathematically, Eq. (S16) can be rewritten in a more compact form as $\Gamma_{ij}(z) = \sum_{|y_l|<1} C(y_l) e^{-|x_{ij}|/\xi_l} e^{ik_l x_{ij}}$, which is a superposition of exponential functions. When the spin's frequency lies within the band $\omega_0 = \omega(k)$, there exist poles in the unit circle and the integral should be done above the real axis ($z = \omega_0 + i0^+$). It is clear that the contributions from such poles are oscillatory solutions expressed as $\sum_l \gamma_l e^{ik_l(\omega_0)x_{ij}}$ ($|y_l| = e^{-1/\xi_l} = 1$), in keeping with that in the 1D standard bath. However, for band-edge-induced part (analogous to $\omega_0 \neq \omega(k)$), the poles are all inside or outside the integral circle, making the self-energy decay by summing several exponentials ($\xi_l > 0$) [10].

Entangled state preparation

The chiral phonons channel can enable quantum state transfer and entangled states preparation. In this section, we prepare unique entangled steady states via a quasi-unidirectional phonon channel, following closely in Ref. [11]. Though the quasi-chiral interactions can do this too, it requires a more careful treatment of optical dissipation (since the optical fraction of the polaritons at k_2-mode is large). We drive every spins by classical fields at a common frequency ν with the amplitude Ω_j and the detuning $\delta_j = \omega_{0j} - \nu$, with ω_{0j} the transition frequency of the jth spin. Thus, in the rotating frame with respect to the driving frequency ν and under the rotating wave approximation, the Hamiltonian of spins is transferred to

$$\hat{H}_{\text{spins}} = \sum_{j=1}^{N_s}(-\delta_j/2\hat{\sigma}_z^j + \Omega_j\hat{\sigma}_-^j + \Omega_j^*\hat{\sigma}_+^j). \tag{S17}$$

When neglecting the level shifts and separating the spins by a proper distance such that $(k_1-k_2)x_{ij} = 2\pi n$ (n integer), we can obtain a generalized master equation

$$\begin{aligned}\frac{d\hat{\rho}_s}{dt} &= -i[\hat{H}_{\text{edges}} + \hat{H}_{\text{spins}}, \hat{\rho}_s] + (\gamma_1+\gamma_2)\sum_j D[\hat{\sigma}_-^j]\hat{\rho}_s + \gamma_s\sum_j D[\hat{\sigma}_z^j]\hat{\rho}_s \\ &\quad + \gamma_1(1-\eta_1)\sum_{i>j}([\hat{\sigma}_-^i\hat{\rho}_s, \hat{\sigma}_+^j] + [\hat{\sigma}_-^j, \hat{\rho}_s\hat{\sigma}_+^i]) + \gamma_2(1-\eta_2)\sum_{i<j}([\hat{\sigma}_-^i\hat{\rho}_s, \hat{\sigma}_+^j] + [\hat{\sigma}_-^j, \hat{\rho}_s\hat{\sigma}_+^i]),\end{aligned} \tag{S18}$$

with γ_s the spins dephasing rate and $D[\hat{O}]\hat{\rho}_s = \hat{O}\hat{\rho}_s\hat{O}^\dagger - \frac{1}{2}\hat{O}^\dagger\hat{O}\hat{\rho}_s - \frac{1}{2}\hat{\rho}_s\hat{O}^\dagger\hat{O}$ for a given operator $\hat{O}$. Here, $\hat{H}_{\text{edges}} = g_s\sum_j(\hat{\sigma}_j\hat{\sigma}_{j+1}^\dagger + \text{H.c.})$ is the coherent interaction only retained up to the nearest-neighbour. The factor of $1-\eta_{1,2}$ are to model the propagation losses in optomechanical waveguide for respectively right- and left-moving excitation, with $\eta_{1,2} \sim N_p\kappa_C \sin^2\theta_{k_{1,2}}/v_g^{1,2}$ the amplitudes that get loss between the spins, N_p the number of traveled cavities and κ_C the decay rate of the optical cavities. For the quasi-unidirectional channel in this system, $\sin^2\theta_{k_1} \sim 0.003$ can be realized, leading to a low optical loss $\eta_1 \sim 0.01$. Note that if the value of γ_2/γ_1 is small enough such that we can exclude the last term in Eq. (S18), the condition $(k_1-k_2)x_{ij} = 2\pi n$ is not necessary.

Ideally, the dynamics evolution can be towards a pure entangled steady-state when the detuning pattern is designed in pairs, for instance, one with the detuning $\delta_i = \delta_1$ and another with the detuning $\delta_j = -\delta_1$. Here, we assume the frequency difference is tiny enough such that spins are identical with regard to reservoir interaction. In the simplest case of two spins coupled to the bath, the target state has the form of [11, 12]

$$|\psi_{\text{dimer}}\rangle = \frac{1}{\sqrt{1+|\alpha|^2}}(|gg\rangle + \alpha|S\rangle), \tag{S19}$$

with $\alpha = 2\sqrt{2}\Omega_0/[i(\gamma_1-\gamma_2) + 2\delta_1]$ and the singlet $|S\rangle = (|eg\rangle - |ge\rangle)/\sqrt{2}$. The time scale of system to reach the steady state is

$$\tau = \frac{\pi[(\gamma_1-\gamma_2)^2/4 + \delta_1^2 + 2\Omega_0^2]}{(\gamma_1+\gamma_2)[(\gamma_1-\gamma_2)^2/4 + \delta_1^2]}. \tag{S20}$$

We numerically plot the fidelity using Eq. (S18) in Fig. S6(a), where the spin dephasing effect, waveguide loss and band-edge-induced coherent interaction are taken into account. We show the high fidelity is still available. We note that high fidelity does not mean high concurrence since high concurrence requires larger pumping strength Ω_0 which, however, gives rise to longer time to reach the steady state (see Eq. (S20)). Actually, for the parameters used in Fig. S6(a), the concurrence of ideal target state is about 0.68 while the concurrence of the steady state under realistic conditions is about 0.59.

Further, we study the situation where the number of coupled spins is increased to four. There are two cases, one is to form two dimers with the detuning profile $(\delta_1, -\delta_1, \delta_2, -\delta_2)$ and the dark state $|\psi_{\text{dimer}}^{(12)}\rangle|\psi_{\text{dimer}}^{(34)}\rangle$, the other is to

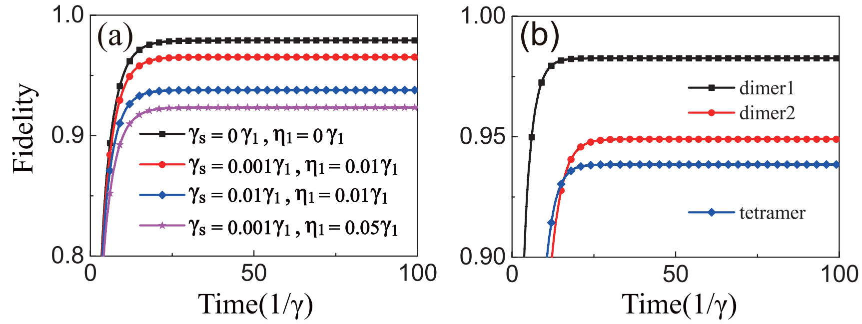

FIG. S6. (Color online) (a) Time evolution of the fidelity with different noise strength (η_1, γ_s) when $(\delta_1, \delta_2) = (0, 0)\gamma_1$. (b) Time evolution of the fidelity for four spins at (η_1, γ_s)=(0.01,0.001)γ_1. Two dimers at $(\delta_1, \delta_2, \delta_3, \delta_4) = (0.4, -0.4, 0.4, -0.4)\gamma_1$ (the black and red lines). A tetramer at $(\delta_1, \delta_2, \delta_3, \delta_4) = (0.6, 0.4, -0.6, -0.4)\gamma_1$ (the blue line). Here, Ω_j=0.5γ_1, γ_2=0.02γ_1, $\eta_2 = 1$, $g_s = 0.01\gamma_1$.

form a four-particle entangled state with the detuning profile $(\delta_1, \delta_2, -\delta_1, -\delta_2)$ (or $(\delta_1, \delta_2, -\delta_2, -\delta_1)$) and the dark state [11]

$$\begin{aligned}|\psi_{\text{tetramer}}\rangle \propto\ & |gggg\rangle + a_{12}|S\rangle_{12}|gg\rangle_{34} + a_{34}|S\rangle_{34}|gg\rangle_{12} \\ & + a_{13}(|S\rangle_{13}|gg\rangle_{24} + |S\rangle_{14}|gg\rangle_{23} + |S\rangle_{23}|gg\rangle_{14} + |S\rangle_{24}|gg\rangle_{13}) \\ & + a_{1234}|S\rangle_{12}|S\rangle_{34} + a_{1324}(|S\rangle_{13}|S\rangle_{24} + |S\rangle_{14}|S\rangle_{23}). \end{aligned} \tag{S21}$$

In terms of $Z \equiv -i(\gamma_1 - \gamma_2)/2$, the five coefficients read

$$a_{12} = \frac{-\Omega_0[2Z^2 + 2\delta_1\delta_2 - (Z + \delta_1)(\delta_1 + \delta_2)]}{\sqrt{2}(Z - \delta_1)^2(Z - \delta_2)} \tag{S22}$$

$$a_{34} = \frac{-\Omega_0(Z - \delta_1 + \delta_2)}{\sqrt{2}(Z - \delta_1)(Z - \delta_2)} \tag{S23}$$

$$a_{13} = \frac{\Omega_0(\delta_1 + \delta_2)}{2\sqrt{2}(Z - \delta_1)(Z - \delta_2)} \tag{S24}$$

$$a_{1324} = \frac{-2\sqrt{2}\Omega_0 a_{13}}{2Z - \delta_1 - \delta_2} \tag{S25}$$

$$a_{1234} = \frac{\Omega_0^2(\delta_1 + \delta_2 - 4Z)}{(Z - \delta_1)(Z - \delta_2)(\delta_1 + \delta_2 - 2Z)}. \tag{S26}$$

In Fig. S6(b), we plot the fidelity of these two type of entangled states preparation and show the high fidelity (> 0.9) is realizable in this system under realistic conditions.

BANDGAP REGIME

Photon-phonon bound state and its robustness

When spins' frequency lies within the acoustic bandgap, the bound state can form and exponentially localize in the vicinity of the cavity to which spin is coupled. The bound state is obtained by solving $\hat{H}|\psi\rangle = E_{BS}|\psi\rangle$, with $\hat{H} = \hat{H}_{\text{OM}} + \hat{H}_{\text{free}} + \hat{H}_{\text{int}}$, and the general form of the bound state in momentum space

$$|\psi\rangle = (C_e\hat{\sigma}_+ + \sum_k \sum_{\beta=a,b} C_{k,\beta}\beta_k^\dagger)|g\rangle|\text{vac}\rangle. \tag{S27}$$

Here, $|C_e|^2$ is the probability of finding the excitation in spin excited state, which can be obtained by imposing the normalization condition. $C_{k,a}$ and $C_{k,b}$ are photon and phonon distributions of bound state in k-space. The energy of bound state $E_{\rm BS}$ can be solved by pole equation $E_{BS} = \omega_0 + \Sigma_e(E_{BS})$, with Σ_e the self-energy[13]. After some algebra, we arrive to the following expression

$$C_{k,a} = g_{\rm eff} C_e \big(-\frac{\sin\theta_k \cos\theta_k}{E_{\rm BS} - \omega_u(k)} + \frac{\sin\theta_k \cos\theta_k}{E_{\rm BS} - \omega_l(k)} \big) \tag{S28}$$

$$C_{k,b} = g_{\rm eff} C_e \big(\frac{\cos^2\theta_k}{E_{\rm BS} - \omega_u(k)} + \frac{\sin^2\theta_k}{E_{\rm BS} - \omega_l(k)} \big). \tag{S29}$$

We focus on the specific situation where the middle bound state forms. If choosing $E_{\rm BS} = 0$, the conditions $C_{k,a} = C_{k+\pi,a}$ and $C_{k,b} = -C_{k+\pi,b}$ are satisfied regardless the value of θ we choose, as discussed before. The wave function distributions of bound state in real space can be obtained by fourier transform

$$C_{j,a/b} = \frac{1}{2\pi} \int_{-\pi}^{\pi} dk e^{ikj} C_{k,a/b}. \tag{S30}$$

Since there is no singularity, we can integrate it directly. Intuitively, when $j = 2n$ (n integer), $e^{i(k+\pi)j} C_{k+\pi,a} = e^{ikj} C_{k,a}$ and $e^{i(k+\pi)j} C_{k+\pi,b} = -e^{ikj} C_{k,b}$. The situation is opposite when $j = 2n+1$. Thus we obtain the main feature of this bound state that the photon and phonon components are alternating, i.e., $C_{2n,b} = 0$ and $C_{2n+1,a} = 0$. Actually, it takes advantage of the feature of cosine function. Moreover, if the bands are asymmetry when $\theta \neq \pi$, the distributions in real space can acquire a tunable phase (as a result of the asymmetric band structure), which can also be understood from the formula ($C_{k,a/b} \neq \pm C_{-k,a/b}$).

We also consider the robustness of this exotic bound state by plotting the phonon component of bound state. First, for varying spins' frequency around the optimal value, the bound state is still robust when $\omega_0 \lesssim 0.1\varepsilon$, as shown in Fig. S3(c). Second, the off-diagonal and on-site disorder are considered, which are shown in Fig. S3(a) and S3(b). We show that the middle bound state is robust against two type of disorders and the feature of alternating photon and phonon components of the bound state is robust against off-diagonal disorder.

Tunable odd-neighbor spin-spin interactions

When considering the situation that two or multiple SiV centers are coupled to the optomechanical crystal, the bound state can mediate spin-spin interactions, which can be harnessed to simulate spin models. The dynamics in Markovian limit is described in Eq. (S11). Since $\omega_0 \neq \omega_{u/l}(k)$, $\Gamma_{ij} = -(\Gamma_{ji})^*$ and we can simplify the Eq. (S11) to (using Eq. (S13) and Eq. (S14))

$$\frac{d\hat{\rho}_s}{dt} = \sum_{i,j} -\Gamma_{ij}(\omega_0)[\hat{\sigma}_+^j \hat{\sigma}_-^i, \hat{\rho}_s]. \tag{S31}$$

It shows coherent spin-spin interactions with a coupling strength of $-i\Gamma_{ij}(\omega_0)$. Comparing Eq. (S12) with Eq. (S29), we show the spin-spin interactions are indeed mediated by the phonon component of the bound states. Since the bound state is alternating for photon and phonon components, the mediated spin-spin interactions is odd-neighbor.

There are several applications in quantum simulation and quantum information processing such as the simulation of spin models, state transfer and long-distance entanglement of many qubits through an auxiliary one (the auxiliary spin in odd site and others in even sites).

Besides, we also consider the tunability of the localization length of this long-range interactions with respect to the system parameters θ, G, K. The ratios of the coupling strength of the first four interacting spins are shown in Fig. S7, which reflects the localization length. We show the localization length can be tuned and made larger by closing the bandgap, where we fix G, K and vary θ or fix θ, K and vary G, as shown in Fig. S7(a) and S7(b). Also, a short localization length involving only nearest-neighbor spins can achieve when fixing the values of G, J and reducing the value of phonon hopping rate K, as shown in Fig. S7(c).

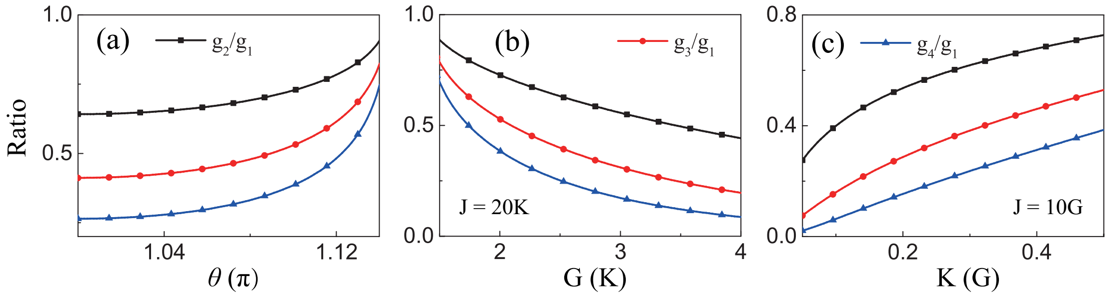

FIG. S7. (Color online) The ratios of the coupling strength of the first four interacting spins. (a) $J = 20K$ and $G = 2K$ are fixed while θ varies from π to 1.14π. (b) $J = 20K$ and $\theta = 1.1\pi$ are fixed while G varies from $1.5K$ to $4K$. (c) $J = 10G$ and $\theta = 1.1\pi$ are fixed while K varies from $0.05G$ to $0.5G$.

Bound states and spin interactions in a finite optomechanical array

In the Markovian limit, we predict the spin-spin coupling strength as $g_{ij} = -i\Gamma_{ij}(\omega_0)$, or equivalently as $g_{ij} = g_{\text{eff}}C_{j-i,b}/C_e$. The first expression can only be calculated with periodic boundary conditions, while the second expression is also applicable to the case of open boundary conditions. Here, we consider a finite optomechanical array with size $N = 7$ and $N = 41$, for $\theta = 1.1\pi$, respectively. We label the cells from the left to right as $-(N-1)/2, -(N-1)/2+1, \cdots, 0, \cdots, (N-1)/2$ such that the laser phase in the middle nanocavity is $e^{-i*0*\theta}$ for symmetry. We first focus on the case of a single spin placed in the middle nanocavity. We find the exotic spin-polariton bound state with alternating photon and phonon components persists, even in an optomechanical array with small size, as shown in Fig. S8(a,d). The energy of the bound state is the same as the bare spin and is robust against to spin-phonon coupling strength [14], which can be verified by solving $\hat{H}|\psi\rangle = \omega_0|\psi\rangle$ for $N = 7$, with $\hat{H} = \hat{H}_{\text{OM}} + \hat{H}_{\text{free}} + \hat{H}_{\text{int}}$ (see concrete expressions in Eq. (S1), Eq. (S8) and Eq. (S9)). This bound state can mediate odd-neighbor and complex spin-spin interactions. Figures S8 (a) and (d) display the bound state with alternating photon and phonon components.

In the following, we exam the spin interactions in Eq. (8) beyond the Markovian approximation. Without loss of generality, we first consider three spins coupled to the mechanical modes of three middle nanocavities ($j = 0, \pm 1$) and single excitations in the system with the ansatz

$$|\psi(t)\rangle = (C_{1,-1}(t)\hat{\sigma}_+^1 + C_{2,0}(t)\hat{\sigma}_+^2 + C_{3,1}(t)\hat{\sigma}_+^3)|ggg\rangle|\text{vac}\rangle + \sum_{j=-(N-1)/2}^{(N-1)/2}\sum_{\beta=a,b} C_{j,\beta}(t)\hat{\beta}_j^\dagger|ggg\rangle|\text{vac}\rangle, \tag{S32}$$

where $|C_{i,j}(t)|^2$ is the probability of spin i being in the upper state with subscript j denoting the position of spin at the optomechanical array, and $|ggg\rangle$ represents three spins being in the lower level. Within Markovian approximation, the dynamics is governed by odd-neighbor and complex spin-spin interactions modeled as

$$\hat{H}_s = g_{12}(\hat{\sigma}_+^2\hat{\sigma}_-^1 + \hat{\sigma}_+^3\hat{\sigma}_-^2) + g_{12}^*(\hat{\sigma}_+^1\hat{\sigma}_-^2 + \hat{\sigma}_+^2\hat{\sigma}_-^3), \tag{S33}$$

with $g_{12} = g_{\text{eff}}C_{1,b}/C_e = g_{32}^*$. As discussed in the main text, this approximation is valid in the weak-coupling limit $g_{\text{eff}} \ll K$. To exam the validity, we plot the time evolution of probability $|C_{i,j}(t)|^2$ in Fig. S8(b,c) for $N = 7$ and in Fig. S8(e,f) for $N = 41$, with $g_{\text{eff}}/K = 0.1$ and the initial state $|\psi(0)\rangle = \hat{\sigma}_+^2|ggg\rangle|\text{vac}\rangle$. The exact spin dynamics is directly calculated by using $\hat{H}$, as shown in Fig. S8(b,e). As a comparison, the Markovian dynamics dominated by Eq. (S33) is given in Fig. S8(c,f). We show the exact evolution is in line with the prediction from the Markovian approximation. Thus, for the parameters used in the main text, the Markovian approximation is valid.

To see the properties of the spin interactions more clearly, we now investigate the case of five spins placed in the

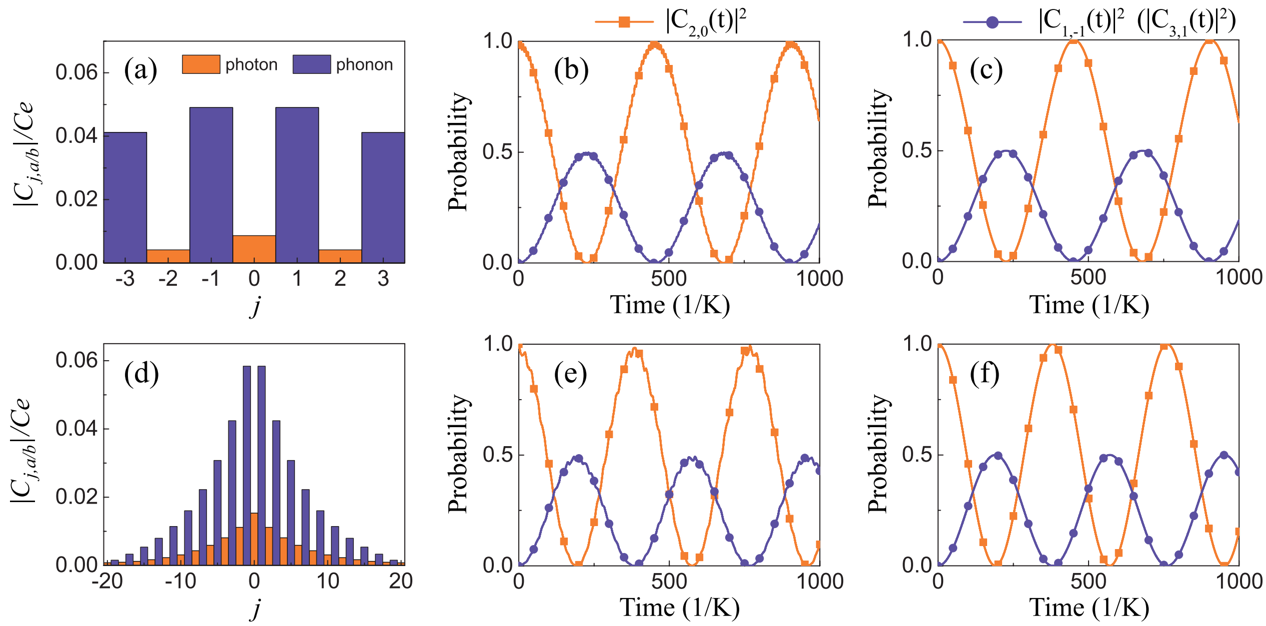

FIG. S8. (Color online) Bound state and spin interactions in a finite optomechanical system with (a,b,c) $N = 7$ and (d,e,f) $N = 41$. (a,d) Photon-phonon bound state with energy $E_{\rm BS} = \omega_0 = \omega_M$, which can be used to predict spin-spin coupling strength as $g_{ij} = g_{\rm eff}\, C_{j-i,b}/C_e$. (a) and (d): The bound state with alternating photon and phonon components. (b,c,e,f): Dynamics of three spins resonant with the middle three mechanical modes, with $|C_{i,j}(t)|^2$ the probability of spin i (at the jth lattice site) being in the upper state. The spin's dynamics is governed by (b,e) total Hamiltonian $\hat{H} = \hat{H}_{\rm OM} + \hat{H}_{\rm free} + \hat{H}_{\rm int}$ and (c,f) spin interactions $\hat{H}_s$ (Eq. (S33)), with $g_{\rm eff} = 0.1K$ and initial state $|\psi(0)\rangle = \hat{\sigma}_+^2|ggg\rangle|\text{vac}\rangle$. Here, we set $\theta = 1.1\pi$, $J = 20K$ and $G = 2K$.

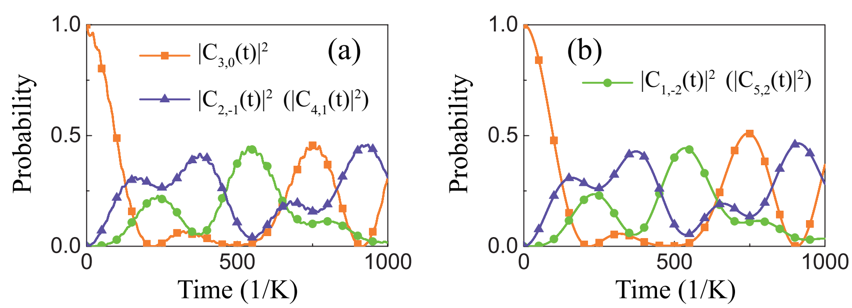

FIG. S9. (Color online) Dynamics of five spins resonant with the middle five mechanical modes of a finite optomechanical system with $N = 41$. $|C_{i,j}(t)|^2$ is the probability of spin i (at the jth lattice site) being in the upper state. (a) Non-Markovian dynamics governed by total Hamiltonian $\hat{H} = \hat{H}_{\rm OM} + \hat{H}_{\rm free} + \hat{H}_{\rm int}$. (b) Markovian dynamics governed by $\hat{H}_s^2$ (Eq. (S35)). Here, $g_{\rm eff} = 0.1K$, $|\psi^2(0)\rangle = \hat{\sigma}_+^3|ggggg\rangle|\text{vac}\rangle$, $\theta = 1.1\pi$, $J = 20K$ and $G = 2K$.

middle five cavities of a $N = 41$ optomechanical array. The single-excitation ansatz is

$$|\psi^2(t)\rangle = (C_{1,-2}(t)\hat{\sigma}_+^1 + C_{2,1}(t)\hat{\sigma}_+^2 + C_{3,0}(t)\hat{\sigma}_+^3 + C_{4,1}(t)\hat{\sigma}_+^4 + C_{5,2}(t)\hat{\sigma}_+^5)|ggggg\rangle|\text{vac}\rangle + \sum_{j=-(N-1)/2}^{(N-1)/2} \sum_{\beta=a,b} C_{j,\beta}(t)\hat{\beta}_j^\dagger|ggggg\rangle|\text{vac}\rangle, \tag{S34}$$

and the Markovian dynamics is governed by the effective Hamiltonian

$$\hat{H}_s^2 = g_{12}(\hat{\sigma}_+^2\hat{\sigma}_-^1 + \hat{\sigma}_+^3\hat{\sigma}_-^2 + \hat{\sigma}_+^4\hat{\sigma}_-^3 + \hat{\sigma}_+^5\hat{\sigma}_-^4) + g_{14}(\hat{\sigma}_+^4\hat{\sigma}_-^1 + \hat{\sigma}_+^5\hat{\sigma}_-^2) + \text{H.c.}, \tag{S35}$$

with $g_{12} = g_{\rm eff}\, C_{1,b}/C_e$ and $g_{14} = g_{\rm eff}\, C_{3,b}/C_e$. Clearly, this Hamiltonian does not involve interactions between even-neighbor spins. We plot spin dynamics both within and beyond the Markovian approximation in Fig. S9, with $g_{\text{eff}}/K = 0.1$ and the initial state $|\psi(0)\rangle = \hat{\sigma}_+^3|ggggg\rangle|\text{vac}\rangle$. Also, the agreement between Fig. S9(a) and Fig. S9(b) indicates that the Markovian approximation is valid.

* lipengbo@mail.xjtu.edu.cn

[1] J. Chan, A. H. Safavi-Naeini, J. T. Hill, S. Meenehan, and O. Painter, Optimized optomechanical crystal cavity with acoustic radiation shield, Appl. Phys. Lett. **101**, 081115 (2012).

[2] G. S. MacCabe, H. Ren, J. Luo, J. D. Cohen, H. Zhou, A. Sipahigil, M. Mirhosseini, and O. Painter, Nano-acoustic resonator with ultralong phonon lifetime, Science **370**, 840 (2020).

[3] A. Seif, W. DeGottardi, K. Esfarjani, and M. Hafezi, Thermal management and non-reciprocal control of phonon flow via optomechanics, Nat. Commun. **9**, 1207 (2018).

[4] M. Schmidt, V. Peano, and F. Marquardt, Optomechanical metamaterials: Dirac polaritons, gauge fields, and instabilities, arXiv:1311.7095.

[5] M.-A. Lemonde, V. Peano, P. Rabl, and D. G. Angelakis, Quantum state transfer via acoustic edge states in a 2D optomechanical array, New J. Phys. **21**, 113030 (2019).

[6] S. Sokolov, J. Lian, E. Yüce, S. Combrié, A. D. Rossi, and A. P. Mosk, Tuning out disorder-induced localization in nanophotonic cavity arrays, Opt. Express **25**, 4598 (2017).

[7] M. Sumetsky and Y. Dulashko, Snap: Fabrication of long coupled microresonator chains with sub-angstrom precision, Opt. Express **20**, 27896 (2012).

[8] M.-A. Lemonde, S. Meesala, A. Sipahigil, M. J. A. Schuetz, M. D. Lukin, M. Loncar, and P. Rabl, Phonon networks with silicon-vacancy centers in diamond waveguides, Phys. Rev. Lett. **120**, 213603 (2018).

[9] H.-P. Breuer and F. Petruccione, *The theory of open quantum systems* (Oxford University Press, 2002).

[10] E. Sánchez-Burillo, D. Porras, and A. González-Tudela, Limits of photon-mediated interactions in one-dimensional photonic baths, Phys. Rev. A **102**, 013709 (2020).

[11] H. Pichler, T. Ramos, A. J. Daley, and P. Zoller, Quantum optics of chiral spin networks, Phys. Rev. A **91**, 042116 (2015).

[12] K. Stannigel, P. Rabl, and P. Zoller, Driven-dissipative preparation of entangled states in cascaded quantum-optical networks, New J. Phys. **14**, 063014 (2012).

[13] C. Cohen-Tannoudji, J. Dupont-Roc, G. Grynberg, and P. Thickstun, *Atom-photon interactions: Basic processes and applications* (Wiley Online Library, 1992).

[14] L. Leonforte, A. Carollo, and F. Ciccarello, Vacancy-like dressed states in topological waveguide QED, Phys. Rev. Lett. **126**, 063601 (2021).